RSC Advances

ROYAL SOCIETY OF CHEMISTRY

www.rsc.org/advances

Abstract

Friction and wear behavior of ultra-nanocrystalline diamond (UNCD) films are sensitive to the phase composition mainly graphite and amorphous carbon (a-C) occupying grain boundaries of sp^3 hybridized diamond nanocrystals. A large volume fraction of grain boundary phase was observed when the diamond was grown in CH_4 (6%)/N_2 plasma medium, and this film exhibited reduced hardness. However, grain boundary phase suppressed and harder sp^3 hybridized volume fraction of nanocrystals dominated in CH_4 (1%)/Ar plasma grown film. Two distinctly different friction and wear behaviors were observed in these films while sliding against a ZrO_2 ceramic ball. High wear and mechanical deformation of ZrO_2 ball were seen while sliding against the hard film and wear loss from the film was rather marginal. In contrast, in case of soft film, the wear loss from the film was found to be significantly higher with the ball being marginally deformed. Such behavior is explained by hard and soft contact combinations composed of ball and film interface. Wear is easy when lamellar graphite structure is dominating in the film, which gets depleted by shear force. Very high friction coefficient up to 0.6 and high wear loss at the beginning of the sliding cycles were observed in these films. This is explained by a residual layer of graphite and a-C contaminated by oxygen functional groups. Interestingly, friction coefficient reduced to the super-low value 0.008 with wearless properties once contaminated layer was delaminated and sliding exhibited with saturated sp^3 rich phase. This was detected in X-ray photoelectron spectra obtained from the wear tracks formed at different sliding distances. A mechanochemical model is proposed to reveal run-in period friction/wear behavior which largely depends on the chemical interaction of the oxidized interfaces.

Keywords: Ultra-nanocrystalline diamond film; super-low friction; interfacial wear; interface mechanochemistry

1. Introduction

Low friction and high wear resistance are the primary requirements for any sliding devices for longer lifetime and enhanced tribo-mechanical efficiency of cutting tools, mechanical assembly component and bio-devices[1-4]. Biocompatibility with low friction and wear of material is one of the most important criteria for biomedical application such as joint prostheses and in other medical applications where the problem of wear and tear of bio-organs is of prime concern.[4]. Moreover, maintaining the sustainability of low friction is necessary for the microelectromechanical system (MEMS) including a biomedical application for precise and trouble-free operation.[1-4] This is possible if wear and deformation of the sliding system are considerably reduced. Minimization of the wear is directly related to the low friction and this can be achieved by designing the material possesses surface inertness and low roughness.[5-8] In this aspect, carbon in the amorphous and crystalline phases is quite suitable to improve above-mentioned properties. In the carbon based phases, most critical compositional variables from the tribology point of view are the distribution of carbon hybridization states and hydrogen content.[9-12] Tailoring the microstructure and phase segregation lead to superior mechanical and tribological properties of nanocrystalline/amorphous carbon-based nanocomposite coatings.[13] It is understood that plasma chemistry is the defining factor to control the grain size and the volume fraction of amorphous carbon (a-C) occupying grain boundary in nanocrystalline diamond (NCD) and ultra-nanocrystalline diamond (UNCD) films.[14,15] Grain size, orientation, chemical composition, volume fraction of grain boundaries and surface morphology are crucial intrinsic material properties needed to tailor the wear and friction in nanostructured diamond films. Above-mentioned characteristics of the films can be tailored by optimizing and controlling the plasma species and post chemical treatment. The ultra-low friction coefficient and superior

wear resistance were obtained via optimization of chemical species, microstructure and morphology of UNCD nanowire films treated in ionized hydrogen and oxygen plasma medium.[16,17] It was observed that UNCD nanowire film, mainly consist of ultra-nanocrystalline diamond grains with $sp^2C=C$/a-C bonded grain boundaries.[15,18] However, the grain boundary volume fraction significantly reduced after H_2/O_2 plasma treatment and film possessed a large fraction of ultra-nanodiamond grains.[16,17] In these films, the low friction coefficient is attributed to the passivation of carbon dangling bonds and adsorption of atmospheric H_2O molecules.[10,17,19-21] In ambient atmospheric condition, ceramic ball such as Al_2O_3, ruby and Si_3N_4, including steel ball showed low value of friction coefficient sliding against UNCD film[22]. However, SiC ball sliding with UNCD film generates high value of friction coefficient. C.S. Abreu et al showed self-polishing mechanism accomplished by diamond asperities truncation when NCD film slide against diamond coated counterbody[23]. The friction evolution of the self-mated tests starts with a sharp peak arising from mechanical interlocking between the diamond asperities. A subsequent transition regime of running-in, corresponding to the accommodation between counterbodies, leads to a final steady-state regime where ultra low friction coefficient was observed. Nevertheless, friction and wear mechanism in UNCD film are not yet completely understood due to complex attributes of grains and grain boundaries. Moreover, a transformation of sp^3 to sp^2 and amorphous structure further complicate the understanding of friction and wear behavior. It is rather a poorly investigated subject, especially in macro-contacting scale of tribological condition where surface defects, tribolayer formation, chemical transformation, chemical ageing, and mechanochemistry together play an important role to influence friction/wear behavior.

Based on this background, present paper attempts to investigate tribological mechanism of two different UNCD films deposited in (a) CH_4 (1%)/Ar and (b) CH_4 (6%)/N_2 plasma medium.

These films were characterized by several techniques including high-resolution transmission electron microscope (HR-TEM). A wide range of macro-tribometric loads was used to reveal the trend in friction and wear behavior. Deformation and damage of the exposed sliding contacts were studied to propose a relationship between load dependent friction and wear. Graphite and diamond phases were analyzed to reveal the wear mechanism in two different types of UNCD films. Raman and XPS measurements of the wear tracks were systematically carried out to investigate the structural and chemical changes appeared in different sliding regimes. Wear and friction mechanisms were proposed based on mechanochemical model dealing with deformation and accompanying structural/chemical changes of sliding system. The tribochemical product evolved during the run-in period was analyzed and correlated with the operating friction and wear modes.

2. Experimental section

The UNCD films were grown on mirror polished silicon (100) substrates in a microwave plasma enhanced chemical vapor deposition (MPECVD) system (2.45 GHz 6″ IPLAS-CYRANNUS). Before the deposition, the substrates were ultrasonicated in a methanol solution containing a mixture of nanodiamond powder (~5 nm) and titanium powder (325 nm) for 45 minutes to facilitate the generation of surface sites for nucleation. The UNCD film was deposited using CH_4 (1%)/Ar plasma with a microwave power delivery of 1200 W, a pressure of 120 Torr and a substrate temperature of 450˚C. The other UNCD film was deposited in CH_4 (6%)/N_2 plasma with a microwave power of 1200 W, a pressure of 50 Torr and a substrate temperature of 700˚C. For simplicity, films deposited in CH_4 (1%)/Ar and CH_4 (6%)/N_2 plasma medium will be designated as UNCD(Ar) and UNCD(N) film, respectively throughout this manuscript. Both samples were grown over a 30 minutes duration by maintaining the flow rate of gases at 100

sccm. The selected parameter is optimized for the growth of equiaxed diamond grains in Ar

atmosphere whereas nitrogen atmosphere was used for the growth of needle-like

morphology[24,25]. There are several factors, including difference in ionization potential of inert

gases (Ar and nitrogen) which greatly influence the nucleation and growth of diamond film. For

the ideal growth condition, the ionization potential determines the effective pressure of reactive

gases and substrate temperature. Overall, inert gas, pressure and optimized temperature condition

tailors the morphology, microstructure, and chemical composition of the UNCD film. The

morphologies and microstructures of these films were examined using a field emission scanning

electron microscope (FE-SEM, Zeiss Supra 55) and a transmission electron microscopy (TEM;

Jeol 2100; 200 kV), respectively. The surface topography and roughnesses of these films were

analyzed using an atomic force microscope (AFM, Park XE-100). The local chemical structure

of film surface and wear tracks were examined using a Raman spectrometer (Renishaw inVia,

Model NVIA, wavelength 514.5 nm). The surface chemical structure of the film was investigated

using X-ray photoelectron spectrometer (XPS, ESCALAB 250). The monochromatic X-ray

beam with a diameter of 250 μm enabled the assessment of chemical characteristics both from

the surface and the wear tracks. The hardness and elastic modulus of films were evaluated by a

nanoindentation (Triboindenter TI 950, USA) coupled with Berkovich diamond indenter with a

tip curvature of 150 nm. A maximum load of 6 mN and a loading-unloading rate of 1.5

mN/minute were used. To avoid any substrate effect, the maximum penetration depth of

indentation was well below the 1/10 of the film thickness. The friction and wear behavior of

these films were measured by a ball-on-disc tribometer (CSM, Switzerland) operating in a linear

reciprocating mode. A ZrO_2 ball with 6 mm diameter and ~45 nm roughness was used as a

sliding counterbody. The standard hardness and elastic modulus of the ZrO_2 ball is 12 and 200

GPa, respectively. At 2 N load, the Hertzian stress of UNCD(Ar) and UNCD(N) film against 6 mm spherical ZrO_2 ball is 0.8 GPa and 0.73 GPa, respectively. Calculation was carried out considering the Poison ratio 0.201[24] and 0.23 for UNCD film and ZrO_2 ball, respectively. The elastic modulus of UNCD(Ar) and UNCD(N) film is 215 GPa and 165 GPa, respectively. A stroke length of 4 mm, sliding speed 4 cm/s and data accusation rate of 10 Hz was used during each experiment. The tests were carried out in ambient (dry and unlubricated) conditions. Three-dimensional wear profiles in both films were obtained from a Taylor Hobson 3D profilometer. The damage of the wear tracks and the ball scars were examined by an optical microscope.

3. Results and discussion

3.1 Morphology, microstructure and chemical characteristics of UNCD films

The FE-SEM micrographs shown in Figure 1(a) and (c) reveal the morphology of the UNCD(Ar) and UNCD(N) films, respectively. The UNCD(Ar) film contains equiaxed diamond grains whereas the UNCD(N) film exhibits needle-like morphology.[15,25] This observation is well supported by AFM topography, which for UNCD(Ar) film shows the distribution of fine particles with an average surface roughness of 9.4 nm (Figure 1(b)). However, in case of UNCD(N) film, diamond particles are encapsulated into wire-like features with an increased surface roughness of 13 nm (Figure 1(d)). The thicknesses of the UNCD(Ar) and UNCD(N) films are ~1.8 and ~1.2 μm, respectively, and these values were obtained from FE-SEM cross-sectional analysis. Figure 2(a) shows a typical TEM image of the UNCD(Ar) film, depicting the uniform distribution of equiaxed particulates.
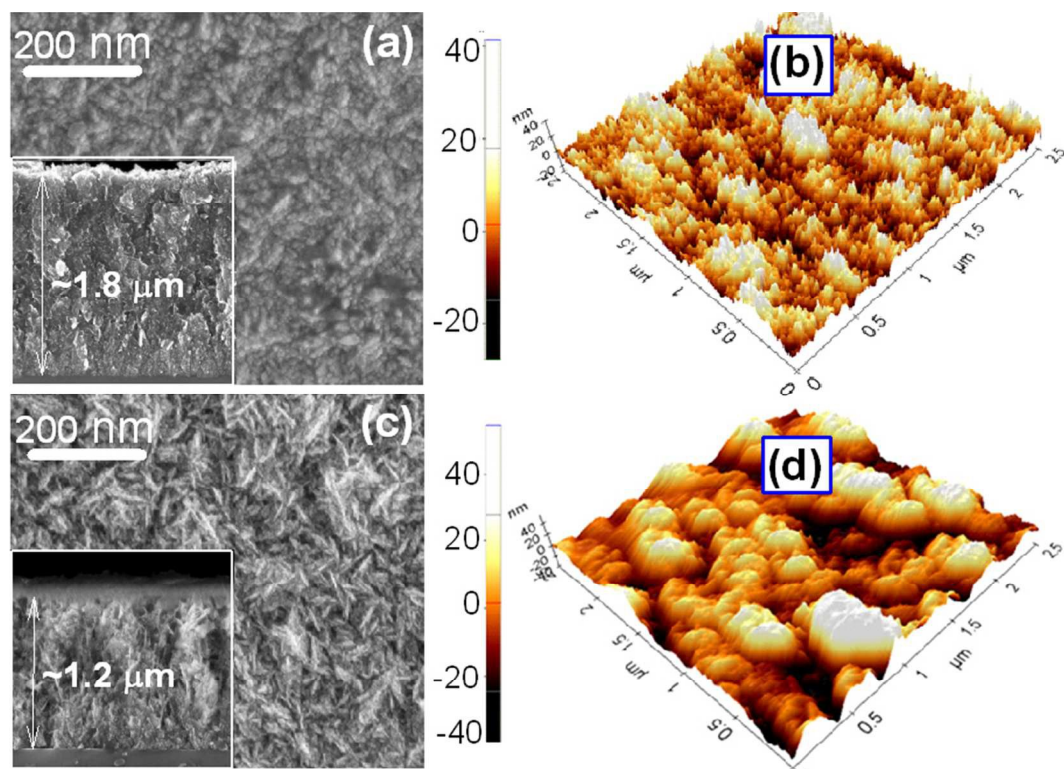
Figure 1. Surface morphology and topography of (a-b) UNCD(Ar) and (c-d) UNCD(N) films, cross section image is given in SEM images

Selective area electron diffraction (SAED) pattern is shown in the inset of Figure 2(a), have sharp diffraction rings corresponding to (111), (220) and (311) planes of the diamond lattice. Furthermore, the lattice plane spacing of (311), (220) and (111) are estimated to be 0.11, 0.12, and 0.21 nm, respectively, which are in agreement with the crystalline diamond structure[25], thereby confirming that these particulates are nanocrystalline diamonds. The diffused ring in the center of SAED pattern indicates the presence of a-C/sp^2 bonded phase. The HRTEM image (Figure 2(b)) of the UNCD(Ar) film is obtained from the marked area 'A' in Figure 2(a). It reveals that the particulates observed in Figure 2(a) are actually the aggregates of ultra-small diamond grains and the diamond aggregates are uniformly distributed throughout the film. Fourier transformed image (FT_{01}) in the inset of Figure 2(b) contains discrete diffraction spots

8

corresponding to diamond grains and the central diffused ring is evident of a-C/sp^2 bonded phase. The existence of diamond and a-C phases are highlighted by FT images ft$_1$ and ft$_2$, respectively, which correspond to regions 1 and 2, respectively (Figure 2(b)). Figure 2(c) shows a typical TEM micrograph of UNCD(N) film. The SAED exhibits ring-shaped pattern corresponding to (111), (220) and (311) diamond lattice.
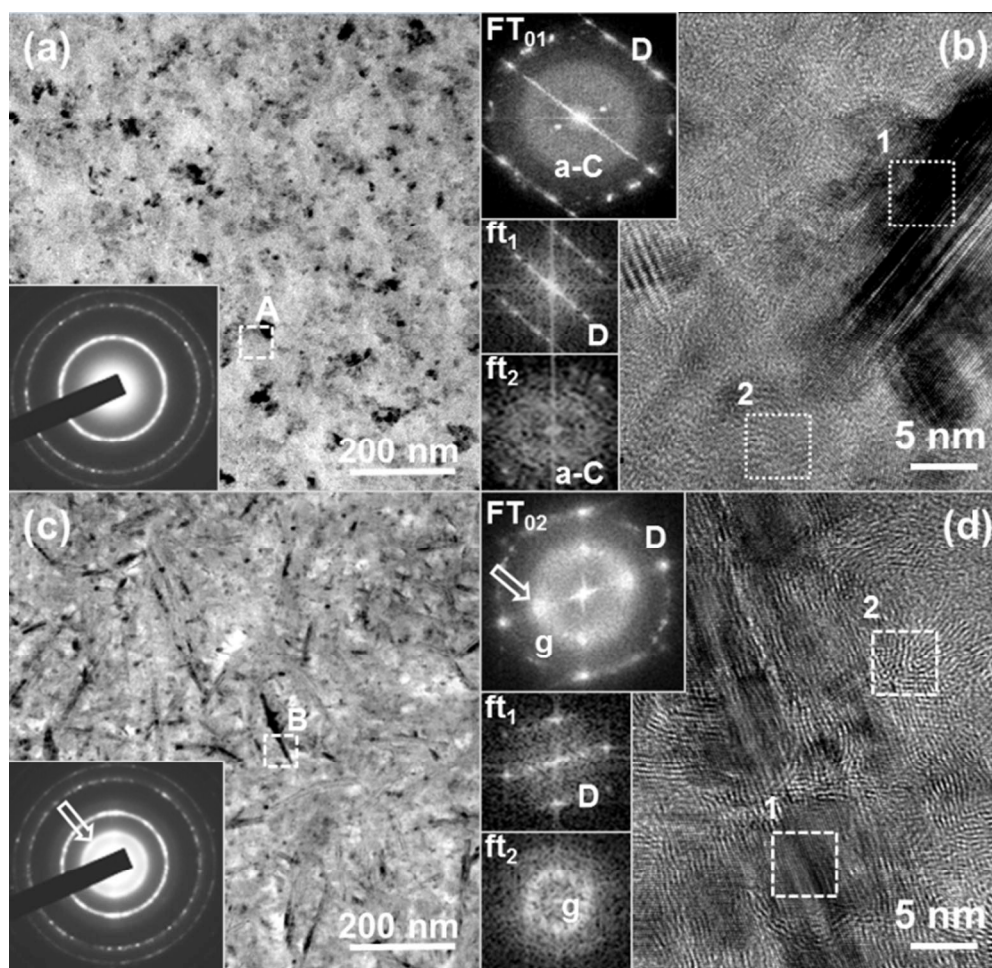

Figure 2. TEM and HRTEM images of UNCD(Ar) film (a) and (b), respectively, UNCD(N) (c) and (d)

This implies that the wire-like particulates observed in the TEM image are randomly oriented diamond grains. Prominent diffraction ring, which is located inside the (111) diamond ring in the

9

center of the SAED pattern (indicated by arrow in Figure 2(c)), signifies the existence of graphite

phase in UNCD(N) film. Figure 2(d) shows the structural image of the film obtained from area

'B' marked in Figure 2(c). Fourier-transformed FT_{02}-image of the whole structure image of

Figure 2(d) shows a spotted diffraction pattern arranged in a ring shape, a characteristic of the

diamond phase. However, there exist strong diffraction spots in FT_{02} lying along a ring of

smaller size than a diamond ring (indicated by arrow) also, which indicates the presence of

graphite phase. In addition, region 1 with the FT image ft_1 in the HR-TEM image corresponds to

wire-like diamond grains, whereas region 2 with FT image ft_2 belongs to graphite phase. The

HR-TEM image confirms the growth of diamond in wire-like structures surrounded by graphite

phase. Nanowires are composed of several segments rather than a continuous structure and

exhibit atomically sharp interfaces separated by structural defects, possibly twin boundaries.[18]

The change in surface morphology and grain growth in diamond depends on several factors,

including plasma species.[18, 26-29]

Figure 3(a) and (b) show Raman spectra of UNCD(Ar) and UNCD(N) films, respectively.

Six peaks were observed in the Raman spectra of UNCD(Ar) film. These are v_1, v_2 and v_3 of

trans-polyacetylene (TPA) peaks, refer to the fingerprint of grain boundary phases in

nanodiamond phase.[30-32] The D and G band correspond to sp^2/a-C phase.[33,34] A weak feature of

the D* band at 1333.6 cm^{-1} is a signature of diamond phase.[32] However, in UNCD(N) film, the

D* band is clearly absent and the intensity of v_2 peak is weak, which could be related to the

increase in sp^2/a-C phase in the grain boundaries. The intensity of v_1 and v_3 modes of *TPA* is

decreased in UNCD(N) film, which is clearly related to reduced hydrogen concentration in the

grain boundary. The ratio of the Raman intensities, I(D)/I(G) is 0.35 in UNCD(Ar) and this

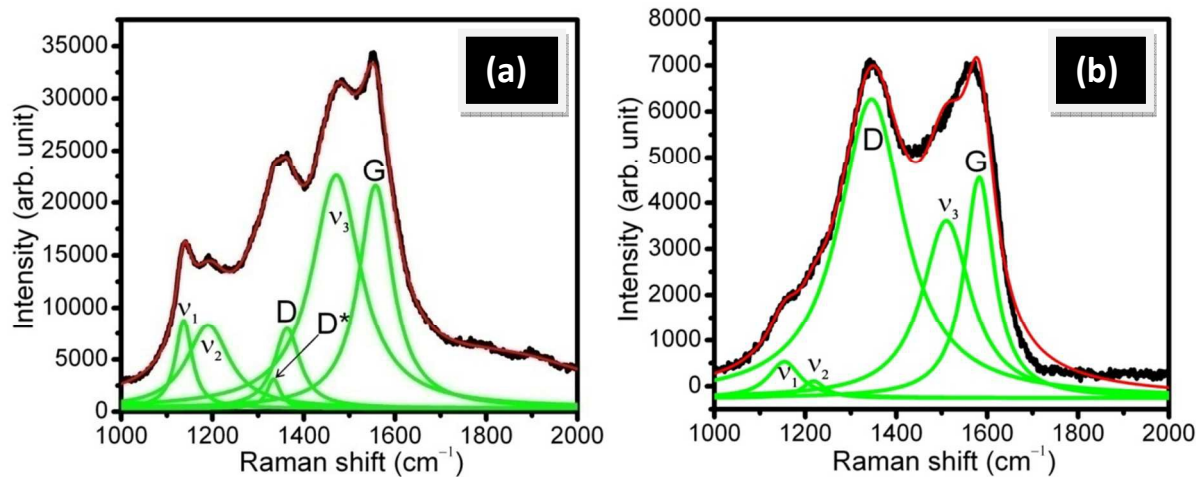significantly increases to a value of 1.38 in UNCD(N) film.

Figure 3. Raman spectra of (a) UNCD(Ar) and (b) UNCD(N) film

The $I(D)/I(G)$ ratio is inversely proportional to crystallite size of the sp^2 domains in the carbon films.[35] The Raman peak of the G band is centered at 1557 cm^{-1} in UNCD(Ar) and shifted to 1582 cm^{-1} in UNCD(N) film, signifying occurrence of more sp^2 carbon domains in the film.[15,18] Above facts describe that sp^2 phase–fraction is enhanced in UNCD(N) film as compared to UNCD(Ar) film.

3.2 Friction and wear behavior

Load dependent friction and wear behavior of UNCD(Ar) film are shown in Figure 4. To obtain the saturated value of friction coefficient, the test was carried out over longer sliding distance. Depending upon the sliding distance, several regimes of friction coefficient ranging from high to ultra-low value were observed. The initial value of friction coefficient was high and increased with increase in the normal load from 1 to 8 N and further declined at highest load of 10 N. Inset shows the average value of friction coefficient with standard deviation, which is high due to higher value of friction coefficient at the beginning of the test.
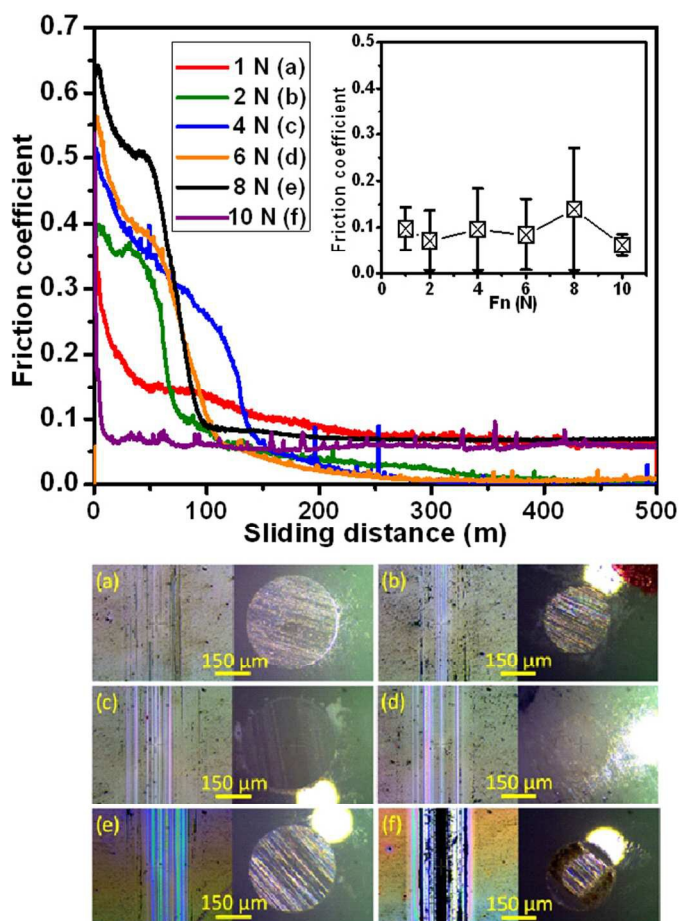
Figure 4. Load dependent friction coefficient and wear of film and ZrO_2 ball sliding against UNCD(Ar) film with constant sliding speed 4 cm/s

However, super-low value (~0.002) is observed after 250 m of sliding distance. Mild deformation of the film is observed while changing loading condition from (a) to (e). However, subsurface deformation with a fractured film surface is observed in loading condition (f). Load dependent friction stability is found to be high and the low value of friction coefficient is maintained even when the film was partially failed at 10 N load. Wear scar dimension is found not to be consistent with the load. Therefore, the load is not being considered a controlling factor for wear. A detailed feature of the wear tracks of (b) and (d) formed at 2 and 6 N loads,

respectively, is given in three-dimensional (3D) images (Figure SI-1). Wear depth in the film is negligible, but the width is large. This is due to wider scar developed on the ball, which leaves behind the sliding mark on the film without inscribing deeper track in the film. Few localized small scale sharp scratches in the track are also observed. Generally, the wear increases with loads, but the results show that the dimension of wear in the film and ball does not follow such a trend. Even at lower loads, the wear of film/ball is comparable to that at higher loads. It is observed that friction is high at initial sliding distances and this region could be a defining factor for producing wear and damage. Therefore, it can be conclusively stated that wear and deformation are related to frictional energy and hence the load is not a decisive factor in this sample. The trend of friction coefficient in UNCD(N) versus sliding distance differs from that of UNCD(Ar) film (Figure 5). In this film, the value of friction coefficient ranging between 0.03 and 0.08 saturates at much earlier sliding cycles and also has a lower standard deviation. Wear width of ball scar formed in UNCD(N) film is much smaller, but the depth is higher compared to UNCD(Ar) film. From the above observation, it is clear that two different types of wear mechanisms operate in these films. In UNCD(Ar) film, the deformation of the ball is significantly high even at low loads and film does not deform much. In contrast, deformation of ZrO_2 ball is marginal when it slides against UNCD(N) film. However, deformation and wear loss of the film are higher. Such a contrasting behavior is explained by considering the hardness of the film-ball combination. In this aspect, hardness values of UNCD(Ar) film and ZrO_2 ball are 23 and 12 GPa, respectively. It can be considered hard and soft sliding combination. In this condition, a softer ball is easily worn-out by plowing while sliding against harder UNCD(Ar) film.[36] However, the hardness of the UNCD(N) film (14.8 GPa) is comparable to the ZrO_2 ball and wear loss through the plowing from the ball is restricted.
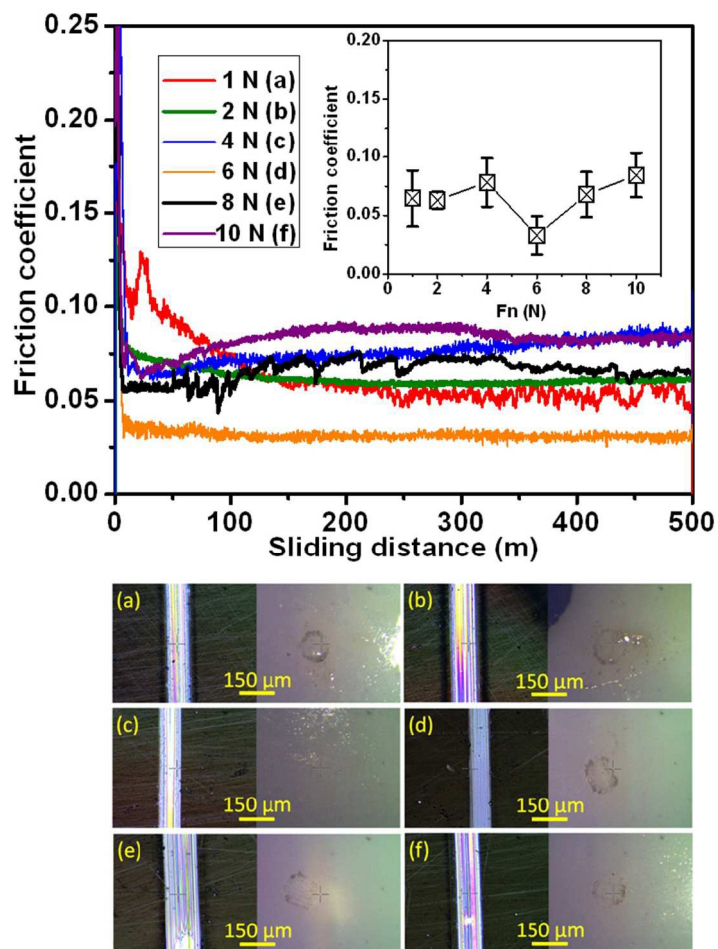
13

Figure 5. Load dependent friction coefficient and wear of film and ZrO$_2$ ball sliding against UNCD(N) film with constant sliding speed of 4 cm/s

The UNCD(N) film contains a large amount of softer phases like graphite and a-C, which easily shear and delaminate exhibiting high wear as compared to that of UNCD(Ar) film. Most important observation points to the high friction regime in the UNCD(Ar) film which exists for long sliding distance and it is a contributing factor for high wear of the ball. Due to the presence of softer phase like a-C in UNCD(N), the film wears more readily than ZrO$_2$ ball. For this film, a 3D image of the wear tracks formed at 2 and 6 N were obtained (Figure SI-2). Here, deeper tracks are formed, but the wear width is less as compared to UNCD(Ar) film. The reason for

such a wear behavior is described by the smaller scar of the ball which points to the higher

magnitude of contact stress leading to more wear of UNCD(N) film. The experimental

observation shows drastic changes in friction coefficient versus sliding distance in both the films.

To distinguish the role of stress in friction and wear of UNCD(Ar) and UNCD(N) films, two

different modes of tribo-experiments were carried out (a) pausing the test for 2 minutes without

changing the ball contact in same wear track (b) fixing the new contact of ball in same wear track

and continuing the test after two minutes of pause. In mode (a) of tribo-experiment on

UNCD(Ar) film, several pauses were periodically made during the test for approximately two

minutes (Figure SI-3). The high magnitude of friction peak is clearly seen when the test is

continued after each pause. The value abruptly increases to a higher magnitude and gradually

saturates after 4 to 5 m of sliding distance. At each pause, the dimension of the ball is analyzed

and it is found to be nearly same. In the mode (b), several fresh contacts were established during

the test under similar loading and sliding conditions as used in Figure SI-3. The friction behavior

is more or less similar, but the dimension of the scar formed on the ball extensively differs

(Figure SI-4). After the pause of 20 and 76 m of sliding distances, the scar is seen to be much

larger as shown in optical images of (a) and (b). In this region, the friction coefficient is found to

be quite high and this is capable of generating additional damage and wear from the ball. In the

region spanning from 76 to 132 m, the friction coefficient is small and it is in the saturation

stage. This directly corresponds to the marginal increment in the scar dimension. Consequently,

the deformation at sliding distance (c) is smaller compared to that observed at (a) and (b). The

dimension of the ball scar is further decreased and it is nearly similar at the distance from (d) to

(h). In this entire region, the friction coefficient is low and does not differ much. From this

analysis, it is clearly pointed out that most of the wear and deformation of the ball occur during

initial sliding cycles when the dissipation of frictional energy is high. Moreover, friction coefficient does not clearly depend on contact area or stress. If the periodic peak is due to high stress, then it should not appear in case when the contact position of the ball is not changed and the stress remains same as compared to previous cycles (Figure SI-3). A similar test is performed on UNCD(N) film following the mode (a) and (b). Similar to the UNCD(Ar) film, the jump in friction coefficient is observed in UNCD(N) film and it gradually saturates after certain sliding distance (Figure SI-5). The dimension of the ball scar is almost the same after each pause. Similarly, the test was carried out while fixing the fresh contact after each pause (Figure SI-6). In this condition, the peak in friction is observed and the dimensions inscribed in ball scar are also nearly similar. This clearly points to a fact that the contact stress is not the governing factor for this kind of abrupt jumps in friction coefficient.

3.3 Mechanochemical model of friction and wear

To explain the above problems from chemical and structural points of view, the tribology tests were carried out on UNCD(Ar) film for 30 m and 500 m of sliding distances (Figure 6(a)). Two distinctly different values of friction coefficient with high and ultra-low magnitudes were recorded. Raman spectra were obtained from these wear tracks to examine the changes in chemical structure and carbon bonding configuration (Figure 6(b)). Intensity, shape, size, and peak position of v_1, v_2, v_3, D*, D and G bands show similarity at both positions pertaining to a lapse of 30 m and 500 m of sliding distances. All these parameters are also comparable to that of Raman spectra obtained from the film surface as shown in Figure 3(a). The intensity ratio I(D)/I(G) in wear tracks is 0.32±0.03, which is very close to 0.35 observed from the UNCD(Ar) film surface. The analysis confirms that the chemical structure and bonding configuration of the wear tracks remain stable and unchanged during the sliding process.
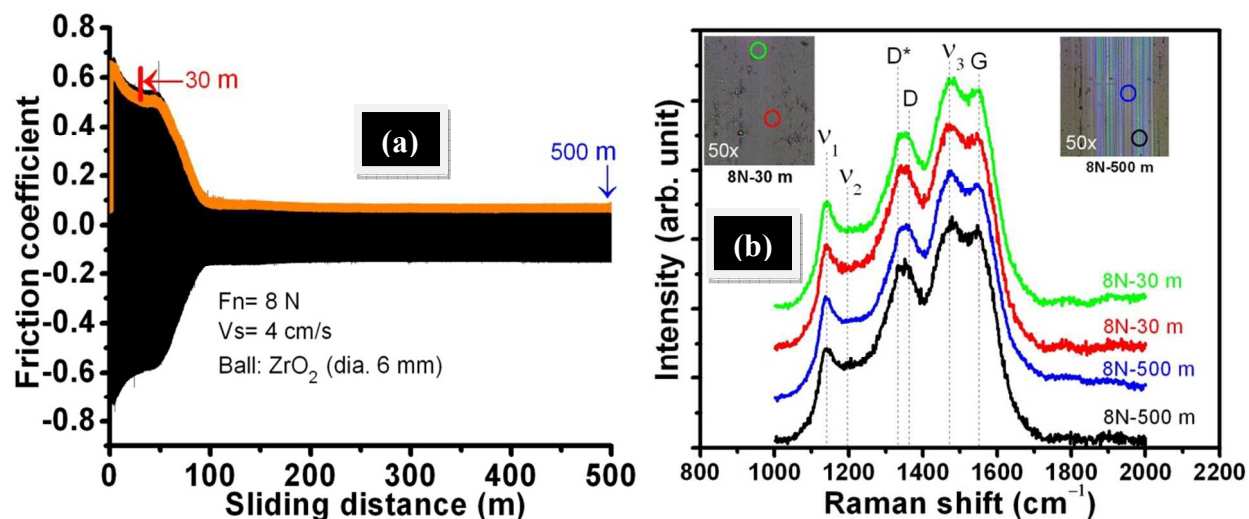
Figure 6. Friction coefficient (a) and Raman spectra (b) obtained from the wear track of UNCD(Ar) film at different sliding distance of 30 m and 500 m

On the basis of this result, high and ultra-low values of friction coefficient at two different sliding locations could not be explained by Raman spectra. In the wear tracks of UNCD(N) film, the v_1, v_2 and v_3 peaks related to *TPA* are disappearing due to the sliding process (Figure 7). I(D)/I(G) ratio decreased to 0.99 and 1.02 in the wear track at a sliding distance of 2.5 m and 500 m, respectively. This fact clearly indicates that the chemical structure of the film has slightly changed during initial sliding cycles and remains same up to 500 m of sliding distance. Decrease in I(D)/I(G) ratio and shifting of G peak position at 1578 cm^{-1} correspond to the ordering of carbon lattice.[32,34] The ordering of carbon structure is the same in the wear track formed at 2.5 and 500 m of sliding distances. However, the corresponding values of friction coefficient significantly differ. Raman analysis of wear tracks obtained from these spots corresponding to high as well as super-low friction coefficients does not show visible chemical changes and is unable to explain such a large difference in friction behavior. Therefore, UNCD(N) film was

17

selected for further detailed XPS analysis to investigate the difference in friction coefficient and wear on the basis of local chemical changes.
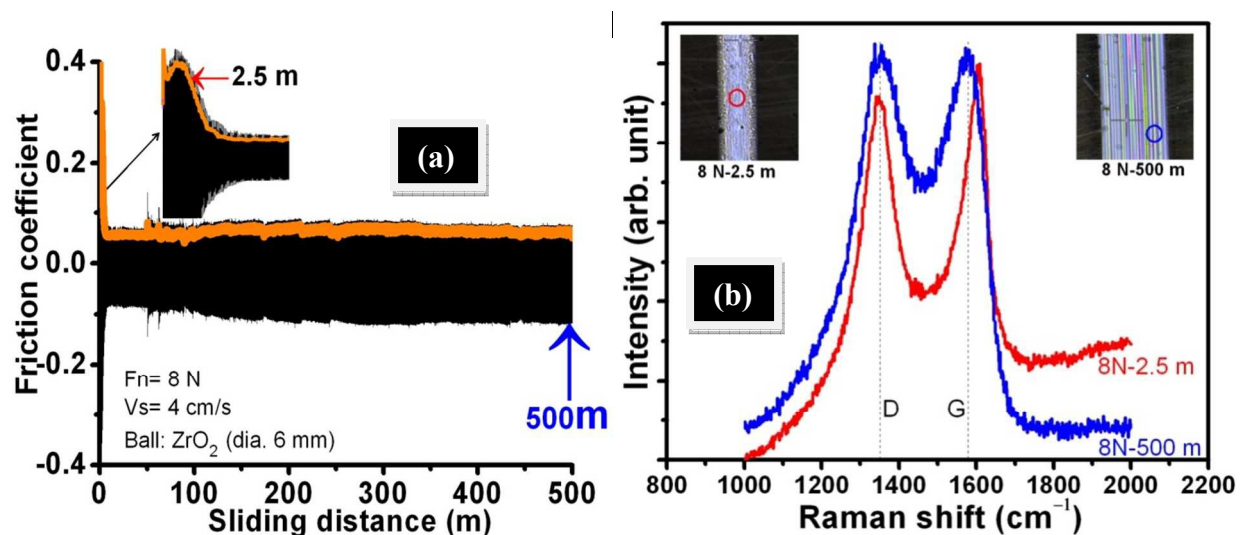

Figure 7. Friction coefficient (a) and Raman spectra (b) obtained from the wear track of UNCD(N) film at different sliding distance of 2.5 m and 500 m

XPS spectra were obtained systematically from the wear tracks formed at the sliding distance of 2 m and 100 m. These results were compared with the XPS spectra obtained from the film surface. For this purpose, the tribo-experiment was carried out at 2 N load and 4 cm/s sliding speed. This belongs to friction curve (b) shown in Figure 5. It is clearly seen that friction at a sliding distance of 2 m is high ~0.25 which decreases to ~0.05 at a sliding distance of 100 m. The analysis will correlate the change observed in friction coefficients with local chemical changes, which occur in the wear tracks due to sliding. For simplicity, spectra obtained from the (a) film surface, inside the wear track formed at (b) 2 m and (c) 100 m of sliding distances will be further designated as spots (a), (b) and (c), respectively. XPS in Figure 8(a–c) represents survey spectra at the spots (a), (b) and (c). In all the figures, an inset shows an enlarged spectrum

in the energy range of 0-250 eV. It is shown that spot (a) exhibits C 1s, O 1s, Si 2s and Si 2p lines.
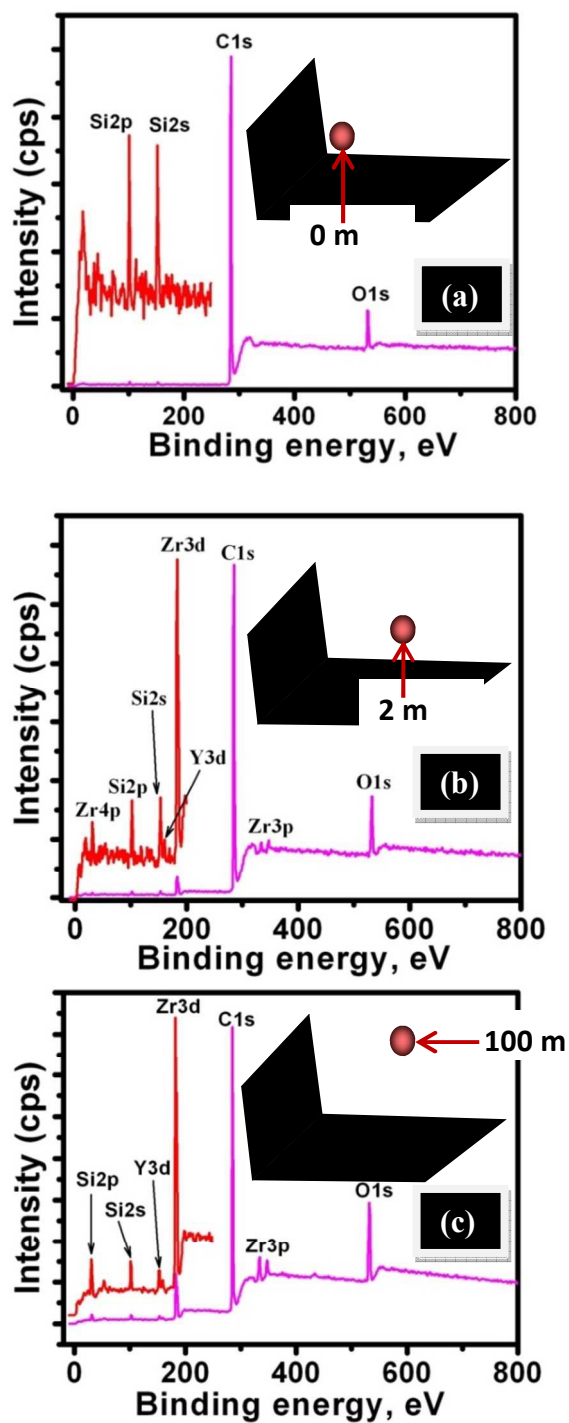

Figure 8. XPS survey spectra at spot (a), (b) and (c) representing film surface and wear track formed at 2 m and 100 m sliding distance, respectively

The small amount of silicon was possibly segregated to the surface during the film deposition. Additional spectral lines such as Zr 4p, Zr 3p, Zr 3d and Y 3d were observed at spots (b) and (c). These peaks belong to wear particles transferred from ZrO_2 ball which get deposited onto the wear track during the friction test. Deposited mass transfer from the ball is maximized at 100 m of sliding distance and this happens due to the supply of continuous mechanical energy. This evidence is shown in an enhanced intensity of the XPS line at a spot (c). The intensity of Si 2s and Si 2p peaks decrease with increase in sliding distance and becomes least at spot (c). This could be related to the deficiency of the segregated silicon, which is mostly present on the film surface and depleted during the sliding process. Yttrium (Y) is present in ZrO_2 ball as an admixture. The oxygen concentration in the wear tracks is increased due to tribo-induced oxidation, which further forms various surface adsorbed functional groups. This aspect is further investigated below in HR-XPS analysis.

The C 1s and O 1s spectra are useful to understand the tribo-chemical and oxidation reaction products accompanying concomitant changes in sp^3/sp^2 ratio on these three spots. These results are presented in Figure 9 and 10, respectively. This will help to draw a friction and wear model based on mechanochemical interaction. The C 1s spectra were deconvoluted into four lines indicated as A, B, C and D components corresponding to certain chemical bonds that exist in the diamond film (Figure 9). Component A with a binding energy around 284.4 eV refers to C=C (sp^2) bonding typically for graphite. Binding energy B around 284.9-285.1 eV refers to tetrahedral C-C (sp^3) bonding in diamond.[37] Component C in the energy range 285.6-285.8 eV is designated as a carboxyl group of C-COO and CH_2COH containing a hydroxyl group OH which exists at all the three spots.[37,38] Molecular fragments containing different ratios in group C-COO,

CH$_2$COH, CH$_2$-O represents component D with a binding energy value spanning 286.6-286.9 eV. The above chemical details are summarized in Table 1.

Figure 9. Deconvoluted HR-XPS of C 1s obtained from the spots (a), (b) and (c) representing film surface and wear track formed at 2 m and 100 m sliding distance, respectively
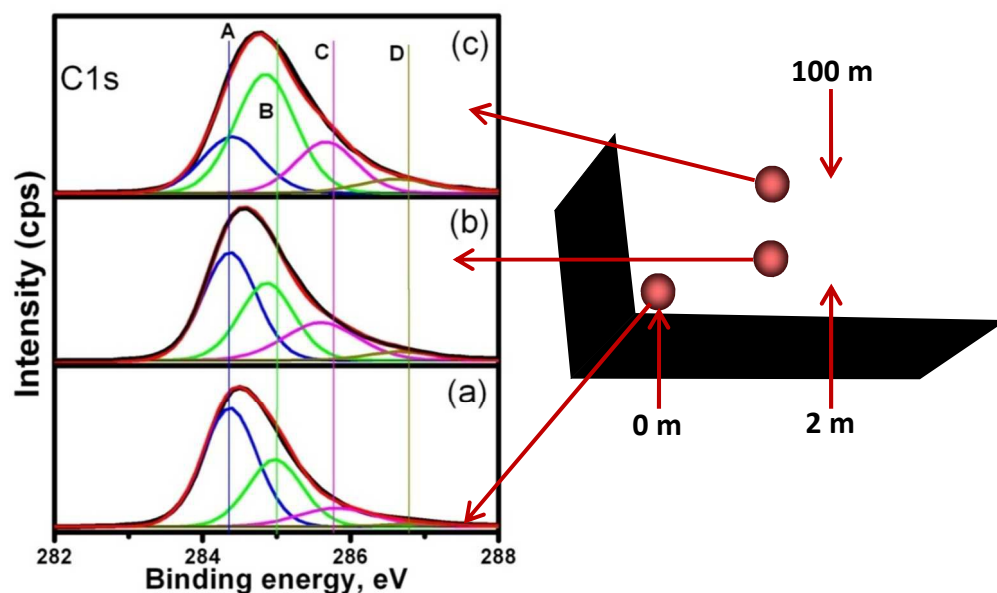

Figure 10. Deconvoluted HR-XPS of O 1s obtained from the spots (a), (b) and (c) representing film surface and wear track formed at 2 m and 100 m sliding distance, respectively
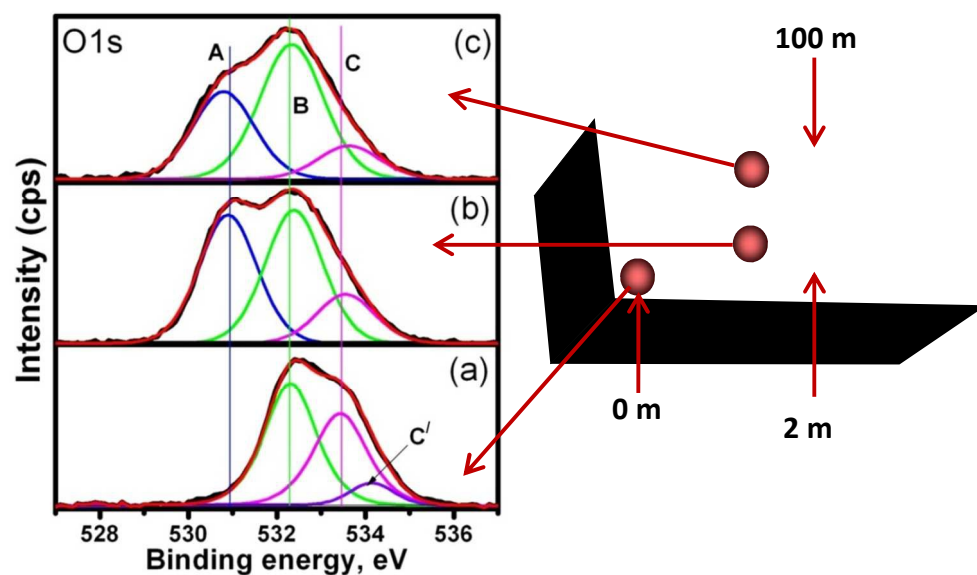
Table 1. The energy components, chemical groups, binding energies and ratio of chemical species of

deconvoluted C 1s lines at spots (a), (b) and (c)

Component	Chemical groups	BE (eV) of C 1s peak		
		spot (a)	spot (b)	spot (c)
A	$C=C$ (sp^2)	284.4	284.4	284.4
B	$C-C$ (sp^3)	285.0	284.9	284.9
C	$C-COO$, CH_2COH	285.8	285.6	285.7
D	$CH_2 - O$	286.9	286.7	286.6
		Ratio of BE obtained from C 1s spectra		
		spot (a)	spot (b)	spot (c)
B/A	----	0.565	0.725	2.107
C/A	----	0.221	0.484	0.908
D/A	----	0.032	0.100	0.323
C/B	----	0.39	0.67	0.43
D/B	----	0.06	0.14	0.15

It is valuable to reveal the chemical nature of O 1s peaks also on these spots. XPS spectra of an

O 1s line at the spots (a), (b) and (c) is shown (Figure 10). These spectra are analyzed for an

interaction of oxygen, carbon and their functional groups on these spots. Energy components,

chemical groups, a range of binding energies, and ratio of deconvoluted peaks are summarized in

Table 2. O 1s and C 1s spectra from the surface of nanoscale catalysts on graphite have been

studied earlier.[39,40] Based on these data, it is validated that component A at a binding energy

(BE) 530.4-530.9 eV at spots (b) and (c) includes carboxylic structures on the surface[37] and this

band is absent at spot (a). The presence of oxygen in carbon corresponds to the energy

component of a carboxyl group of component C (Figure 9). Component B at BE of 532.0±532.4

eV is attributed to the presence of weakly bonded oxygen in the molecular entity with a covalent

bond. The oxygen is a part of the hydroxyl group[41] or typical molecular oxygen species.[39,40] In

the C 1s spectrum, this may correspond to component D. At all these spots, chemical component

C indicates the presence of OH group centered at BE range 533.4–533.4 eV. Finally, component

$C^/$, with BE 534.2 eV indicates the presence of OH group and water at a spot (a). These chemical

species belong to adsorbed contaminated surface layer and it does not appear at spots (b) and (c) due to the erosion of this layer. In addition to the traditional classification [41] component A of ZrO_2 in O 1s spectra occurs due to the wear of ZrO_2 ball surface at the spot (b) and (c).

Table 2. The energy component, chemical groups, binding energies and ratio of chemical species of deconvoluted O 1s lines at spots (a), (b) and (c)

Component	Chemical groups	BE (eV) of O 1s peak		
		spot (a)	spot (b)	spot (c)
A	O from ZrO_2, C-OO, CH_3COH	----	530.9	530.8
B	O from SiO film, weakly bonded oxygen atoms	532.3	532.4	532.3
C	OH- group, SiO_2	533.4	533.5	533.6
C$'$	OH- group, H_2O, SiO_2	534.2	----	----
		Ratio of BE obtained from O 1s spectra		
		spot (a)	spot (b)	spot (c)
A/B	----	----	0.97	0.63
C/B	----	0.78	0.37	0.24
C$'$/B	----	0.15	----	----

The O 1s energy line of ZrO_2 exists at 530.4 eV.[42] The presence of trace amount of SiO_2 at the spot (a) arises on the surface during the film growth process. Silicon may oxidize and form Si-O bond at BE 532.5 eV and this also can result in the formation of possible compounds of silicon and oxygen in the form of SiO_2 in O 1s energy line around 534 eV.[43] This particular chemical shift is not found at spots (b) and (c), which indicates segregation of a small amount of silicon on the film surface during the growth that later erodes out during the course of sliding process. A/B ratio is decreased at the spot (c) indicating a decrease in a ZrO_2 fraction. It is a well known fact that wear of the ball is high at the beginning of sliding process and that is why it shows a large fraction of ZrO_2 at a spot (b). Decrease in C/B ratio from the spot (a) to (c) is related to the

removal of an adsorbed contaminated layer which contains a large amount of OH- groups and oxidized silicon species.

Referring to the Figure 9,10 and Tables 1,2, it is clearly seen that sp^3/sp^2 ratio is smaller with a value 0.565 at a spot (a) and it increases to 0.725 and 2.107 at spots (b) and (c), respectively. This indicates the presence of large amount of the $C=C$ sp^2 graphite bond on the surface of the film, which is progressively eroded. This is schematically shown in Figure 11.
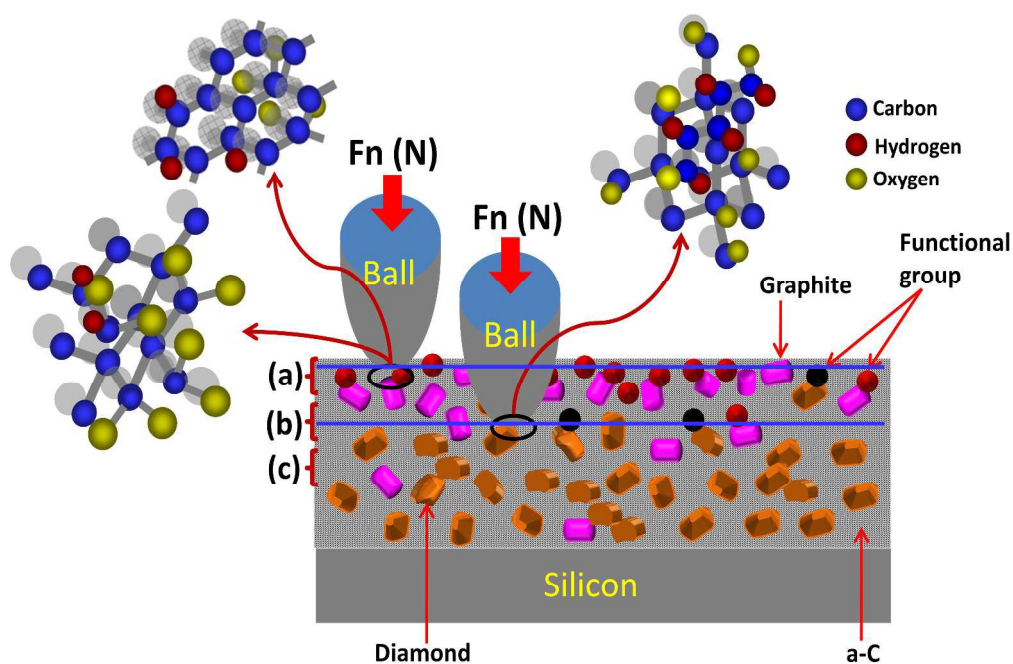

Figure 11. Schematic for wear process in different layer of diamond film based on XPS results and friction data.

In this schematic, the layers (a), (b) and (c) are defined as spots (a), (b) and (c) for XPS analysis. At the surface, the contact interaction is dominated by oxidized a-C/sp^2 carbon. Due to wear process, this layer is removed and contact is mostly influenced by sp^3 hybridized carbon atoms passivated by oxygen bearing functional groups. The large amount of $C=C$ sp^2 on the surface is

related to the growth process of diamond films and the entrained defect, which allows

unsaturated sp^3 bonds to reorient into a distorted sp^2 bond on the film surface, eventually forming

oxygen bearing functionality in the ambient atmosphere.[37] It is noticed that C/A and D/A ratio is

less on the surface of the film at the spot (a) and increases with sliding distances at spots (b) and

(c). In contrast, C/B ratio does not largely differ at spots (a) and (c), but it increases to 0.67 at a

spot (b). It means that high frictional energy supports the formation of functional groups through

oxidation induced by the tribo-chemical reaction. The D/B ratio has the lowest value of 0.06 at a

spot (a) and it increases to 0.14 and 0.15 at spots (b) and (c), respectively. Such increment is also

driven by the tribo-chemical reaction, but it is not related to frictional energy because D/B ratios

are nearly similar at spots (b) and (c), but friction coefficients largely differ on these two spots.

Therefore, removal of sp^2 layers from the surface leads to exposing further sp^3 rich carbon phase.

This behavior is dominated as the sliding is progressed, generating oxygen functionalities due to

tribo-chemical reactions.

The influence of the humidity-induced surface oxidation during the pause of sliding contact

is proven to generate the induction period of so-called "run-in" during which the friction

coefficient is high and it gradually decreases to stabilized ultra-low value of friction coefficient.[44]

During the pause, the sliding interface is exposed for enough time duration to an atmosphere

which brings in interaction with excess O$_2$ and H$_2$O radicals leading to the formation of oxidized

tribolayer. The removal of the oxidized surface layer during the run-in period is fully supported

with the correlation between the run-in behavior in friction measurements and the wear mark on

the ball as investigated by the Marino et al.[44] The life of the run-in period depends on the

chemical stability of oxidized tribolayer. This is more stable in UNCD(Ar) film when the contact

position of the ball is not changed during the pause (Figure 8). The potential energy of a nascent

25

diamond surface containing a lot of dangling chemical bonds is favorable for interaction with O_2 and H_2O radicals leading to the formation of oxidized tribolayer. Now, it is easy to understand why abruptly high friction value appears during the tribo-pause that was observed in both the films. This could be related to interface aging when contact is contaminated, forming chemically oxidized carbon layer. Friction coefficient once again returns to the saturated ultra-low regime when tribo-pause is terminated and sliding is resumed. It means that oxidized carbon layer gets detached due to the wear process. In both these samples, longer life of the run-in period at the beginning of the friction test is due to the presence of oxidized sp^2/a-C tribolayer. Generally, ultra-low friction coefficient of NCD/UNCD film in the presence of humid atmosphere and water vapor is associated with OH and H passivation of sliding surfaces, resulting from the dissociative chemisorptions of H_2O molecules.[21,45,46] The presence of adsorbates like OH and H exhibits repulsive force preventing the formation of covalent bonds across the interface. Further, the passivation decreases the energy of the contacting surfaces and increases their inter-electronic repulsion.[45] However, the role of passivation is poorly influencive to get the low friction and wear behavior when a-C/sp^2 phase fraction is oxidized. In contrast, in amorphous hydrogenated carbon film, carbon onions with a closed spherical shell structure are spontaneously formed on the worn surface in the absence of the hydrogen passivation effect, which further reduce the friction coefficient to an extremely low value.[47]. Therefore, for ultra low friction, only contact passivation is not deterministic factor.

4. Conclusions

Friction and wear properties of two different types of UNCD films sliding against ZrO_2 ball were investigated. These properties depend on the film phase composition, microstructure and contaminated adventitious oxidized layer. Wear of the film was significantly less while high

26

wear from the ZrO_2 ball was observed in UNCD(Ar) film. This trend was opposite in UNCD(N) film, which revealed higher wear from the film and reduced damage in the ZrO_2 ball. This was explained by the hardness of the film, which increased when sp^3 fraction in the film was high as in the case of UNCD(Ar) film. The plowing mechanism of the ZrO_2 ball is intensified when it slid against hard UNCD(Ar) film. However, UNCD(N) film is soft due to the presence of large amounts of sp^2 and a-C phases which easily delaminated by shear deformation. Very high friction and wear were observed at the beginning of the sliding cycles due to the presence of large amounts of contaminated and oxidized layer on the film surface. This layer was more stable in UNCD(Ar) film, hence the high value of friction coefficient extended to longer sliding distances. The ultra-low value of friction coefficient ranging from 0.03 to 0.08 and wearless properties were observed once a-C/sp^2 oxidized layer was worn off. This was substantiated by carrying out the XPS measurements inside the wear tracks at high and ultra-low zones of the friction coefficient. However, friction coefficient increased up to very high value in both the films while making the tribo-pause for a few minutes. This behavior was explained by a chemical aging effect when surfaces in contact were contaminated.

References

1 W. Weiyuan, W. Yuelin, B. Haifei, X. Bin and B. Minhang, *Sens. Actuator* 2002, 97–98, 486–491.

2 O. Auciello and A.V. Sumant, *Diam. Relat. Mater.,* 2010, 19, 699–718.

3 Y. Liao, R. Pourzal, M. A. Wimmer, J. J. Jacobs, A. Fischer and L. D. Marks, *Science* 2011, 334, 1687–1690.

4 R. J Narayana, R. D. Boehma, A. V. Sumant, Mater. Today 2011, 14, 154–163.

5 P. Stoyanov, P. Stemmer, T. T. Järvi, R. Merz, P. A. Romero, M. Scherge, M. Kopnarski, M. Moseler, A. Fischer and M. Dienwiebel, *ACS Appl. Mater. Interf.,* 2013, 5, 6123–6135.

6 X. Liu, J. Yang, J. Hao, J. Zheng, Q. Gong and W. Liu, *Adv. Mater.,* 2012, 24, 4614-4617.

7 L. Pastewka, S. Moser, P. Gumbsch and M. Moseler, *Nature Mater.,* 2011, 10, 34-38.

8 D. Bernoulli, K. Hafliger, K. Thorwarth, G. Thorwarth, R. Hauert and R. Spolenak, *Acta Mater.* 2015, 83, 29–36.

9 J. Philip, P. Hess, T. Feygelson, J. E. Butler, S. Chattopadhyay, K. H. Chen and L. C. Chen, *J. Appl. Phys.* 2003, 93, 2164–2171.

10 A. R. Konicek, D. S. Grierson, P. U. P. A. Gilbert, W. G. Sawyer, A. V. Sumant and R. W. Carpick, *Phys. Rev. Lett.* 2008, 100, 235502–235505.

11 S. Dag and S. Ciraci, *Phys. Rev. B* 2004, 70, 241401–241404.

12 A. C. Y. Liu, R. Arenal, D. J. Miller, X. Chen, J. A. Johnson, O. L. Eryilmaz, A. Erdemir and J. B. Woodford, *Phys. Rev. B* 2007, 75, 205402–205414.

13 S. Zhou, L. Wang, Z. Lu, Q. Ding, S. C. Wang, R. J. K. Wood and Q. Xue, *J. Mater. Chem.,* 2012, 22, 15782–15792.

14 K. J. Sankaran, P. T. Joseph, H. C. Chen, N. H. Tai and I. N. Lin, *Diam. Relat. Mater.* 2011, 20, 232-237.

15 Y. Tzeng, S. Yeh, W. C. Fang and Y. Chu, *Sci. Rep.* 2014, 4, 4531-4537.

16 K. J. Sankaran, N. Kumar, H. C. Chen, C. L. Dong, B. Ashok, S. Dash, A. K. Tyagi, C. Y. Lee, N. H. Tai and I. N. Lin, *Sci. Adv. Mater.* 2014, 6, 1–9.

17 R. Radhika, N. Kumar, K. J. Sankaran, R. Dumpala, S. Dash, M.S.R. Rao, D. Arivuoli, A. K. Tyagi, N. H. Tai and I. N. Lin, *J. Phys. D: Appl. Phys.* 2013, 46, 425304-425313.

18 R. Arenal, P. Bruno, D. J. Miller, M. Bleuel, J. Lal and D. M. Gruen, *Phys. Rev. B* 2007, 75, 195431–195441.

19 J. D. Schall, G. Gao and J. A. Harrison, *J. Phys. Chem. C* 2010, 114, 5321–5330.

20 G.T. Gao, P. T. Mikulski and J. A. Harrison, *J. Am. Chem. Soc.* 2022, 124, 7202–7209.

21 Maria-Isabel De Barros Bouchet, G. Zilibotti, C. Matta, M. C. Righi, L. Vandenbulcke, B. Vacher and M. Jean-Michel, *J. Phys. Chem. C* 2012, 116, 6966–6972.

22. N. Sharma, N. Kumar, S. Dhara, S. Dash, A. Bahuguna, M. Kamruddin, A.K. Tyagi, Baldev Raj, *Tribol. Int.* 2012, 53, 167–178.

23. C.S. Abreu, F.J. Oliveira, M. Belmonte, A.J.S. Fernandes, R.F. Silva, J.R. Gomes, *Wear* 2005, 259, 771–778.

24. M. Mohr, A. Caron,P. Herbeck-Engel, R. Bennewitz, P. Gluche, K. Bruhne, F. Hans-Jorg, *J. Appl. Phys.* 2014, 116, 124308– 124316.

25 K. J. Sankaran, J. Kurian, H. C. Chen, C. L. Dong, C. Y. Lee, N. H. Tai and I. N. Lin, *J. Phys. D: Appl. Phys.* 2012, 45, 365303–365311.

26 A. R. Sobia, Y. Guojun, C. Jianqing, H. Suixia and Z. J. Xingtai, *Appl. Phys.* 2010, 107, 114324–114327.

27 N. Shang, P. Papakonstantinou, P. Wang, A. Zakharov, U. Palnitkar, I. N. Lin, M. Chu and A. Stamboulis, *ACS Nano* 2009, 3, 1032–1038.

28 M. Sternberg, P. Zapol and L. A. Curtiss, *Phys. Rev. B* 2003, 68, 205330–205339.

29 P. W. May and M. N. R. Ashfold, *J. Appl. Phys.* 2007,101, 53115–53123.

30 R. H. Pfeiffer, K. P. Knoll, S. Bokova, N. Salk and B. Gunther, *Diam. Relat. Mater.* 2003, 12, 268–271.

31 C. Castiglioni, M. Tommasini and G. Zerbi, *J. Phil. Trans. R. Soc. Lond. A* 2004, 362, 2425–2459.

32 A. C. Ferrari and J. Robertson, *J. Phil. Trans. R. Soc. Lond. A* 2004, 362, 2477–2512.

33 A. C. Ferrari and J. Robertson, *Phys. Rev. B* 2001, 64, 75414–75427.

34 A. C. Ferrari and J. Robertson, *Phys. Rev. B* 2000, 61, 14095–14107.

35 L. G. Cancado, K. Takai, T. Enoki, M. Endo, Y. A. Kim, H. Mizusaki, A. Jorio, L. N. Coelho, R. Magalhaes-Panigo and M. A. Pimenta, *Appl. Phys. Lett.* 2006, 88, 163106–163109.

36 K. Holmberg, A. Matthews and H. Ronkainen, *Tribol. Int.* 1998, 31, 107–120.

37 F. Mangolini, J. B. McClimon, F. Rose and R. W. Carpick, *Anal. Chem.* 2014, 86, 12258–12265.

38 N. Kumar, R. Radhika, A. T. Kozakov, K. J. Sankaran, S. Dash, A. K. Tyagi, N. H. Tai and I. N. Lin, *J. Phys. D: Appl. Phys.* 2013, 46, 275501–275507.

39 M.G. Mason, *Phys. Rev. B* 1983, 27, 748-762.

40 V. I. Bukhtiyarov, A. V. Carley, L. A. Dollard and M. V. Roberts, *Surf. Sci. Lett.* 1997, 381, 605–608.

41 R. Radhika, N. Kumar, A. T. Kozakov, K. J. Sankaran, S. Dash, A. K. Tyagi, N. H. Tai and I. N. Lin, *Diam. Relat. Mater.* 2014, 48, 6–18.

42 B. M. Reddy, C. Biswajit, I. Ganesh, E. P. Reddy, T. C. Rojas and A. Fernandez, *J. Phys. Chem. B* 1998, 102, 10176–10182.

43 M. Çopuroğlu, H. Sezen, R. L. Opila and S. Suzer, *ACS Appl. Mater. Interf.* 2013, 5, 5875–5881.

44 M. J. Marino, E. Hsiao, Y. Chen, O. L. Eryilmaz, A. Erdemir and S. H. Kim, *Langmuir* 2011, 27, 12702–12708.

45 G. Zilibotti, S. Corni and M. C. Righi, *Phys. Rev. Lett.* 2013, 111, 146101–146105.

46 F.G. Sen, Y. Qi and A.T. Alpas, *Acta Mater.* 2011, 59, 2601–2614.

47. Hui Song, Li Ji, Hongxuan Li, Xiaohong Liu, Huidi Zhou, Weiqi Wang and Jianmin Chen, *RSC Adv.* 2015, 5, 8904–8911.

31

AUTHOR INFORMATION

Corresponding Author

*Email: niranjan@igcar.gov.in, phystribology@gmail.com

Tel.: +91 44 27480500 (ext. 22537)

Fax: +914427480081

Notes

The authors declare that there is no competing financial interest

Graphical abstract